

# Mathematical Modeling and Analysis of HBV and HDV Co-infection Progression with Treatment and Liver Transplantation

Saddam Hussain<sup>1</sup>, Imtiaz Ahmad<sup>2</sup>, Nigar Ali<sup>3</sup>

<sup>[1,2,3]</sup> Department of Mathematics, University of Malakand, Chakdara Dir Lower, 18000, Khyber Pakhtunkhwa, Pakistan

---

## Abstract

*In this paper, a deterministic mathematical model for the dynamics and progression of the co-infection of hepatitis B virus (HBV) and hepatitis delta virus (HDV) in humans is formulated. The model considers the dynamics of infection with HBV, superinfection with HDV, treatments, liver transplantation, and recovery. Qualitative properties of the model, including boundedness, positivity of the solution, and basic reproduction number, are investigated. Further, the local and global stability of the model is analyzed. Sensitivity analysis is carried out to know the key parameters that determine the dynamics of the disease, especially the co-infection rate and the efficiency of treatment and liver transplantation. Numerical simulations will be performed using Runge-Kutta and nonstandard finite difference methods.*

**Keywords:** Liver Transplantation; Mathematical modeling; HBV/HDV Model; Transmission dynamics; Basic Reproductive Number.

---

## 1. Introduction

Hepatitis B Virus and Hepatitis D Virus impose substantial global health burdens, with HBV affecting nearly 296 million people worldwide as of 2019 and answerable for upwards of 820,000 expiries per annum, primarily due to cirrhosis and hepatocellular carcinoma (HCC) [36]. HDV is a defective RNA virus that needs the existence of HBV to replicate, as it develops the HBV surface antigen (HBsAg) for viral assembly and infection of hepatocytes [20]. HDV co-infection leads to more severe liver disease and rapid development to cirrhosis and HCC compared to HBV mono-infection. [17]. Hepatitis refers to liver inflammation and is also called cluster of viral infections that upset the liver, with the most ordinary sorts being hepatitis A, B, and C. Several deadly infectious diseases influence global populations, including hepatitis B [14]. Formerly referred as serum hepatitis, hepatitis B is a severe liver viral illness, caused by the HBV. The virus definitely targets liver cells known as "hepatocytes," leading to inflammation [42]. Hepatitis B is a major public health concern in both advanced and developing nations. Often called the "silent killer" of the liver, hepatitis B can be asymptomatic for many persons [28]. The virus is spread primarily through contact with infected blood or bodily liquids, containing perinatal transmission, unsafe injections, and sexual contact [35]. Although many individuals with hepatitis B cannot reveal signs in the primary phases of infection, specific may experience sudden signs especially, vomiting, yellowing of the skin (jaundice), fatigue, dark urine, and abdominal pain [14]. Once the virus enter the body, it infects hepatocytes in the liver [2].

Transmission of HDV occurs primarily through percutaneous or mucosal exposure to infectious blood or body fluids, sharing common roots with HBV such as sexual contact, intravenous drug use, and vertical

---

*Email addresses:* saddamuom008@gmail.com (Saddam Hussain<sup>1</sup>), iahmaad@hotmail.com (Imtiaz Ahmad<sup>2</sup>), nigaruon@gmail.com (Nigar Ali<sup>3</sup>)

transmission from mother to child [5]. Notably, HDV infection cannot occur without HBV infection, and thus HDV spreads mostly in residents where HBV is endemic or among high-risk groups with ongoing HBV transmission [18]. Generally HDV co-infection contains about 18% of cirrhosis and 20% of HBV-related HCC, which showing its severe medical effect [34]. Clinically, HDV infection can be considered as HBV/HDV co-infection or HDV super infection in chronic HBV moves. The second is associated with chronic HDV persistence and consequently more aggressive liver disease, leading to faster progression to cirrhosis and high threat of HCC [40]. These types of patients have limited facilities of treatment and diagnosis. Presently, the only therapy for HDV is pegylated interferon- $\alpha$ , which has limited competence efficacy and a high decline rate, with nonstop virological reaction attained in less than 30% cured patients [30]. New antiviral agents such as bulevirtide, an entry inhibitor approved in Europe, are helpful in reducing viral burden but long-term cure remains subtle [19]. Liver transplantation as last hope of life, is the perfect treatment for end-stage liver disease due to HBV/HDV co-infection[9]. While transplantation significantly develops survival and quality of life, it is limited by donor availability, high costs, and the risk of post-transplant viral reactivation[15]. The first fruitful Liver Transplantation (LT) was carried out by Dr. Thomas Starzl in 1967, with LT being permitted for general use following a congressional hearing in 1983 [32]. Today, LT is widely used as a life-saving technique for various conditions, such as chronic liver illness, hepatocellular carcinoma, and acute liver failure [33]. In 2021, there were 34,694 LTs performed worldwide, demonstrating a 6.5 % increase from 2020 and a 20 percent increase compared to 2015 [33].

The development of mathematical models for the coinfection of hepatitis B virus (HBV) with hepatitis D virus (HDV) has progressed parallel to developments in virology and infectious disease science. Since the identification of the hepatitis D virus by Mario Rizzetto in 1977, it has been recognized that hepatitis D virus is a defective virus that requires hepatitis B virus surface antigen for replication, leading to a special type of interaction between the two viruses [43]. Mathematical studies have initially considered the case of HBV alone, where models have been based on systems of ordinary differential equations to represent interactions between uninfected cells, infected hepatocytes, and viral particles [44]. One of the initial steps towards the modeling of coinfection was undertaken by de Sousa and Cunha, who presented one of the earliest within-host models that includes HBV and HDV dynamics, along with their dependence relationship and the role of treatments [45]. Later studies have involved more sophisticated compartmental models that consider coinfecting compartments, nonlinear incidence, and proliferation of infected cells [7, 46]. Mathematical modeling provides valuable information and has a significant influence on our understanding of the transmission dynamics and treatment effects on HBV-HDV co-infection. Mathematical models published before have demonstrated the viral kinetics under the effect of therapy [41]; however, models that consider the transmission, treatment, and transplantation of the infected liver from the perspective of the population remain scarce. The nonlinear mathematical model was applied by Mamo *et al.* to investigate the dynamics of HBV-HDV co-infection, the stability of the disease-free equilibrium, and vaccination as a vital intervention measure in controlling the spread of HBV-HDV infection [29]. A number of mathematical models describing the dynamics of the infection have been proposed earlier. Specifically, Aja *et al.* developed a deterministic model of co-infection with consideration of public health measures like awareness, vaccination, and treatment [4]. Additionally, several clinical and epidemiological studies shed light on the mechanisms of interactions between HBV and HDV [8, 34]. As a result, modern mathematical models of HBV-HDV co-infection contain several infectious compartments, different scenarios of treatment, and various stages of the disease.

In spite of the extensive literature on mathematical modeling of the dynamics of HBV and HDV infections, there are still several significant deficiencies in the current models. The first major deficiency concerns the absence of liver transplantation in most models, although it is a key factor in the treatment of advanced stage liver disease associated with HBV-HDV coinfection. Another major deficiency is the lack of consideration for nonlinear interaction between the mono-infected and coinfecting

compartments, which is necessary to take into account the synergism and competition of both viruses. Moreover, coinfection and superinfection scenarios are often not distinguished in existing models, although they have completely different clinical and epidemiological meanings. Furthermore, most of the preceding models are concerned with either viral dynamics inside a host or population dynamics of infection transmission, yet the aspects of treatments, disease progression, and other intervention strategies are often not included. As such, treatment, recovery, and progression to the stages of severe liver disease that would warrant transplantation have not been sufficiently analyzed mathematically. In order to remedy the shortcomings of existing literature, a deterministic compartmental model, expressed as system (1), is introduced to incorporate treatment, liver transplantations, and recovery, as well as nonlinear transmissions among the infected groups. This more sophisticated model would provide a better insight into the dynamics of the disease and its possible control.

The rest of the paper is organized as follows: Section 2 discuss the model formulation. Section 3 presents the feasibility region. Further, Eequilibria and the basic reproduction number are calculated in Sections 4 and 5, respectively. In Sections 6–7, stability analysis is carried out. Section 8 is devoted to the sensitivity analysis, while numerical simulations and results are given in Sections 9–10. Section 11 summarizes he study with public health implications.

## 2. Model Formulation

To better understand the transmission and progression dynamics of Hepatitis B virus and Hepatitis D virus co-infection, we propose a deterministic compartmental model in this article that describes the transmission dynamics of both infections. The total population is classified into six distinct and mutually exclusive classes: susceptible persons ( $S$ ), entities infected with HBV only ( $I_B$ ), persons co-infected with HBV and HDV ( $I_{BD}$ ), persons undergoing treatment ( $T$ ), entities awaiting liver transplant ( $L$ ), and recovered individuals ( $R$ ). Susceptible entities are recruited into the people at a constant rate  $\Lambda$  and may become infected with HBV through contact with either HBV-infected ( $I_B$ ) or co-infected ( $I_{BD}$ ) entities at a transmission rate  $\beta_1$ . Furthermore, HDV transmission arises only in the presence of HBV, so susceptible entities can also gain co-infection directly from contact with co-infected persons at a separate rate  $\beta_2$ . Recovered persons may lose immunity and return to the susceptible class at rate  $\delta$ , while all individuals are subject to natural death at rate  $\mu$ .

HBV-infected individuals ( $I_B$ ) may progress to HDV co-infection through contact with co-infected individuals at a revised rate  $h\beta_2$ , initiate treatment at rate  $\theta_1$ , recover at rate  $\gamma$ , develop severe difficulties leading to liver transplant candidacy at rate  $\omega$ , or decease due to HBV-related causes at rate  $\mu_1$ , in addition to natural death. Persons in the co-infected class ( $I_{BD}$ ) are infected with both HBV and HDV and may begin treatment at rate  $\theta_2$ , progress to liver complications demanding transplant at rate  $\rho$ , or expire due to co-infection-related causes at rate  $\mu_2$ , again with natural death included. Treated individuals ( $T$ ) are those getting antiviral or supportive therapy, and may recover at rate  $\alpha$ , be moved to the liver transplant waiting list at rate  $\tau$ , or die naturally. The liver transplant class ( $L$ ) contains entities in need of or awaiting transplantation, which may result from co-infection ( $I_{BD}$ ), treatment failure ( $T$ ), or HBV-induced liver failure ( $I_B$ ), with transitions occurring at rates  $\rho$ ,  $\tau$ , and  $\omega$ , respectively. Transplant patients may recover at rate  $\sigma$  or die indeed. Recovered persons ( $R$ ) arise from the treatment, liver transplant, or direct recovery from infection, and leaving the system only through natural death.

The graphic diagram is displayed in fig. (1). Upon the transmission dynamics, we suggest the subsequent setup of ordinary differential equations.

Figure 1: The liver transplantation and HBV-HDV Model (1) flow diagram.

$$\left\{ \begin{array}{l} \frac{dS}{dt} = \Lambda - \beta_1 S(I_B + I_{BD}) - \beta_2 S I_{BD} - \mu S, \\ \frac{dI_B}{dt} = \beta_1 S(I_B + I_{BD}) - h\beta_2 I_B I_{BD} - (\gamma + \theta_1 + \omega + \mu + \mu_1) I_B, \\ \frac{dI_{BD}}{dt} = \beta_2 S I_{BD} + h\beta_2 I_B I_{BD} - (\theta_2 + \rho + \mu + \mu_2) I_{BD}, \\ \frac{dT}{dt} = \theta_1 I_B + \theta_2 I_{BD} - (\alpha + \tau + \mu) T, \\ \frac{dL}{dt} = \rho I_{BD} + \tau T + \omega I_B - (\sigma + \mu) L, \\ \frac{dR}{dt} = \gamma I_B + \alpha T + \sigma L - \mu R. \end{array} \right. \quad (1)$$

As initially:  $S(t) \geq 0$ ,  $I_B(t) \geq 0$ ,  $I_{BD}(t) \geq 0$ ,  $T(t) \geq 0$ ,  $L(t) \geq 0$ , and  $R(t) \geq 0$ .

In the next section, we will find non-negativity, the boundedness and the feasible region  $\Omega$ .

### 3. Basic properties of the model

We analyze the non-negativity of the solution, the boundedness and the feasible region  $\Omega$ .

#### 3.1. Positivity of Solutions

**Lemma 3.1.** *Let the initial conditions of system (1) be non-negative, i.e.,  $S(0) \geq 0$ ,  $I_B(0) \geq 0$ ,  $I_{BD}(0) \geq 0$ ,  $T(0) \geq 0$ ,  $L(0) \geq 0$  and  $R(0) \geq 0$ . Then the solutions  $S(t)$ ,  $I_B(t)$ ,  $I_{BD}(t)$ ,  $T(t)$ ,  $L(t)$  and  $R(t)$  remain non-negative for all  $t \geq 0$ .*

*Proof.* We prove the non-negativity of each state variable using standard comparison theorems and the structure of the differential equations in system (1). Starting with the susceptible class:

$$\frac{dS}{dt} = \Lambda - \beta_1 S(I_B + I_{BD}) - \beta_2 S I_{BD} - \mu S.$$

Ignoring the positive terms  $\Lambda$ , we get:

$$\frac{dS}{dt} \geq -(\beta_1(I_B + I_{BD}) + \beta_2 I_{BD} + \mu)S.$$

This gives the differential inequality:

$$\frac{dS}{dt} \geq -\xi(t)S, \quad \text{where } \xi(t) = \beta_1(I_B + I_{BD}) + \beta_2 I_{BD} + \mu \geq 0.$$

Integrating both sides:

$$S(t) \geq S(0) \exp\left(-\int_0^t \xi(s) ds\right) \geq 0.$$

In similar we can have:  $I_B(0) \geq 0$ ,  $I_{BD}(0) \geq 0$ ,  $T(0) \geq 0$ ,  $L(0) \geq 0$  and  $R(0) \geq 0$

Hence, all state variables remain non-negative for all  $t \geq 0$ . □

Next, we will derive the boundness of the system variables.

### 3.2. Boundedness of Solutions

**Lemma 3.2.** *The set  $\Omega = \left\{ (S, I_B, I_{BD}, T, L, R) \in \mathbb{R}_+^6 : 0 \leq S, I_B, I_{BD}, T, L, R \leq N, N(t) \leq \frac{\Lambda}{\mu} \right\}$  a positive invariant and an attracting set for the model (1).*

*Proof.* Adding the equations from model (1), we get

$$\frac{dN}{dt} = \Lambda - \mu(S + I_B + I_{BD} + T + L + R) - \mu_1 I_B - \mu_2 I_{BD}. \quad (2)$$

Simplify the equation we get

$$\frac{dN}{dt} = \Lambda - \mu N(t) - \mu_1 I_B - \mu_2 I_{BD} \leq \Lambda - \mu N(t),$$

this implies that

$$\frac{dN(t)}{dt} \leq \Lambda - \mu N(t),$$

utilizing the Comparison Principle Theorem [27], we obtain

$$N(t) \leq N(0)e^{-\mu t} + \frac{\Lambda}{\mu} (1 - e^{-\mu t}),$$

Hence,  $\lim_{t \rightarrow \infty} \sup N(t) \leq \frac{\Lambda}{\mu}$ .

Thus, we have shown that the solutions of the model (1) eventually are bounded.

So, the biologically feasible region of the model (1) is given by the following set:

$$\Omega = \left\{ (S, I_B, I_{BD}, T, L, R) \in \mathbb{R}_+^6 : 0 \leq S, I_B, I_{BD}, T, L, R \leq N, N(t) \leq \frac{\Lambda}{\mu} \right\}. \quad \square$$

The following section will discuss the points of equilibria of the model.

## 4. Disease-Free and Endemic Equilibrium Points

The model described by system (1) admits two biologically meaningful equilibrium points: the disease-free equilibrium (DFE) and the endemic equilibrium (EE).

### 4.1. Disease-Free Equilibrium

The disease-free equilibrium corresponds to the absence of infection in the population, that is,

$$I_B^0 = I_{BD}^0 = T^0 = L^0 = R^0 = 0.$$

Substituting these values into system (1) and setting the derivatives equal to zero yields the DFE

$$F_0 = (S^0, I_B^0, I_{BD}^0, T^0, L^0, R^0) = \left( \frac{\Lambda}{\mu}, 0, 0, 0, 0, 0 \right). \quad (3)$$

### 4.2. Endemic Equilibrium

The endemic equilibrium represents the persistent presence of the disease in the population and is denoted by  $F^* = (S^*, I_B^*, I_{BD}^*, T^*, L^*, R^*)$ , where all components are positive and satisfy the following

system:

$$\begin{cases} S^* = \frac{\Lambda + \delta R^*}{\beta_1(I_B^* + I_{BD}^*) + \beta_2 I_{BD}^* + \mu}, \\ I_B^* = \frac{\beta_1 S^* I_{BD}^*}{h\beta_2 I_{BD}^* + \gamma + \theta_1 + \omega + \mu + \mu_1 - \beta_1 S^*}, \\ I_{BD}^* = \frac{(\alpha + \tau + \mu)T^* - \theta_1 I_B^*}{\theta_2}, \\ T^* = \frac{\theta_1 I_B^* + \theta_2 I_{BD}^*}{\alpha + \tau + \mu}, \\ L^* = \frac{\rho I_{BD}^* + \tau T^* + \omega I_B^*}{\sigma + \mu}, \\ R^* = \frac{\gamma I_B^* + \alpha T^* + \sigma L^*}{\delta + \mu}. \end{cases} \quad (4)$$

The next section will find out the basic reproduction number of model (1).

## 5. Basic Reproductive Number

We evaluate the basic reproduction number by the next generation method as described in [37, 31, 38], for this we separate the new infected classes  $I_B$ ,  $I_{BD}$  of the model (1). Directing solely on the new infectious terms, and using the notation from model (1), the matrices representing the infection terms,  $F$  and the transfer terms,  $V$  are defined. The right-hand sides of the equations, denoted by the matrix  $F$  for the infection terms and the matrix  $V$  for the rest of transfer terms, are given by:

$$F = \begin{pmatrix} \beta_1 S^0 (I_B + I_{BD}) \\ \beta_2 S^0 I_{BD} \end{pmatrix}, \quad V = \begin{pmatrix} (\gamma + \theta_1 + \omega + \mu + \mu_1) I_B \\ (\theta_2 + \rho + \mu + \mu_2) I_{BD} \end{pmatrix}.$$

In accordance with the method of next generation matrix for deriving the basic reproduction number of new infected sections  $I_B$  and  $I_{BD}$ , the infection matrix and transition matrix are  $F^*$  and  $V^*$  respectively. Upon DFE point  $F_0$ , we have:

$$F^* = \begin{pmatrix} \beta_1 S^0 & \beta_1 S^0 \\ 0 & \beta_2 S^0 \end{pmatrix}, \quad V^* = \begin{pmatrix} \gamma + \theta_1 + \omega + \mu + \mu_1 & 0 \\ 0 & \theta_2 + \rho + \mu + \mu_2 \end{pmatrix}.$$

$$V^{*-1} = \begin{pmatrix} \frac{1}{\gamma + \theta_1 + \omega + \mu + \mu_1} & 0 \\ 0 & \frac{1}{\mu + \rho + \theta_2 + \mu_2} \end{pmatrix}, \quad F^* V^{*-1} = \begin{pmatrix} \frac{S^0 \beta_1}{\gamma + \theta_1 + \omega + \mu + \mu_1} & \frac{S^0 \beta_1}{\mu + \rho + \theta_2 + \mu_2} \\ 0 & \frac{S^0 \beta_2}{\mu + \rho + \theta_2 + \mu_2} \end{pmatrix}.$$

Furthermore, the matrices  $F$  and  $V$  fulfill the criteria outlined in [21]'s predictions (A1) – (A5). By using the next generation matrix computing the spectral range of  $FV^{-1}$ , we can determine the basic reproduction number  $R_0$ , where  $p_1 = \gamma + \mu + \omega + \theta_1 + \mu_1$  and  $p_2 = \mu + \rho + \theta_2 + \mu_2$ .

$$R_0 = \max \left\{ \frac{S^0 \beta_1}{p_1}, \frac{S^0 \beta_2}{p_2} \right\},$$

by putting the value of  $S^0$ , we have  $R_0 = \max \left\{ \frac{\Lambda\beta_1}{\mu p_1}, \frac{\Lambda\beta_2}{\mu p_2} \right\} = \max \{R_{0B}, R_{0BD}\}$ ,

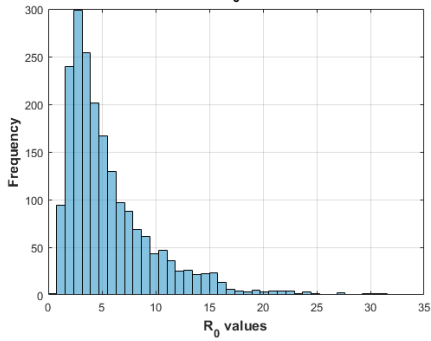
$$R_0 = \frac{\Lambda\beta_1}{\mu p_1} + \frac{\Lambda\beta_2}{\mu p_2} = R_{0B} + R_{0BD}. \quad (5)$$

Where  $R_{0B} = \frac{\Lambda\beta_1}{\mu p_1}$  and  $R_{0BD} = \frac{\Lambda\beta_2}{\mu p_2}$

### 3D Graphs of Basic Reproduction Number $R_0$

Figure 2: Graphical representation of  $R_0$  with effect of various parameters.

SAMPLING.png SAMPLING.png  
Distribution of  $R_0$  (LHS Sampling)



(a) Latin Hypercube Sampling (Bar Chart).

(b) Latin Hypercube Sampling (Scatter Plot).

Figure 3: Comparison of Latin Hypercube Sampling results.

The results in Figure 2 shows that  $R_0$  rises noticeably with higher transmission rates  $\beta_1$  and  $\beta_2$ , demonstrating that stronger transmission mechanisms substantially improve disease spread. In contrast, higher values of the recovery rate  $\gamma$  and the natural mortality rate  $\mu$  decrease  $R_0$ , underlining their role in slowing down infection dynamics. The progression rate  $\theta_1$  exerts a mild positive impact on  $R_0$ , while the disease-induced mortality  $\mu_1$  leads to its decline. Furthermore, increases in the reinfection-related parameters  $\rho$  and  $\theta_2$  result in greater values of  $R_0$ , suggesting that reinfection and advanced-stage transitions strengthen transmission. Figures 3a and 3b grants the sensitivity analysis of the HBV model parameters on the basic reproduction number  $R_0$  using Latin Hypercube Sampling (LHS). The scatter plots validate how variations in parameters such as  $\lambda$ ,  $\mu$ ,  $\beta_1$ ,  $\gamma$ ,  $\theta_1$ ,  $\omega$ ,  $\mu_1$ ,  $\beta_2$ ,  $\rho$ ,  $\theta_2$ , and  $\mu_2$  impact  $R_0$ . Among these,  $\mu$  appears to have a more pronounced inverse relationship with  $R_0$ , signifying its stronger regulatory role in infection spread. The histogram of the  $R_0$  distribution tells that the majority of values are concentrated in the lower range, representing that, under typical parameter deviations, the system generally leftovers in a stable or controlled infection state. This conclusion highlights the inherent robustness of the HBV model and recommends that only substantial changes in perilous parameters can expressively alter the course of disease dynamics

In the following section we will discuss the local and global stability of the DFE points.

## 6. Local and Global Stability of the Disease-Free Equilibrium point

### 6.1. The Local Stability of Disease-Free Equilibrium point

This section will focus on examining the local stability of the DFE point  $F_0$ .

**Theorem 6.1.** For model (1) the disease-free equilibrium (DFE)  $F_0$  is locally asymptotically stable within the feasible region  $\Omega$  when  $R_0 < 1$ .

*Proof.* Using model (1), we have the Jacobian matrix as:

$$J = \begin{pmatrix} m_1 & -\beta_1 S & -(\beta_1 + \beta_2)S & 0 & 0 & 0 \\ \beta_1(I_B + I_{BD}) & m_2 & \beta_1 S - h\beta_2 I_B & 0 & 0 & 0 \\ \beta_2 I_{BD} & h\beta_2 I_{BD} & m_3 & 0 & 0 & 0 \\ 0 & \theta_1 & \theta_2 & -(\alpha + \tau + \mu) & 0 & 0 \\ 0 & \omega & \rho & \tau & -(\sigma + \mu) & 0 \\ 0 & \gamma & 0 & \alpha & \sigma & -\mu \end{pmatrix},$$

where  $m_1 = -\beta_1(I_B + I_{BD}) - \beta_2 I_{BD} - \mu$ ,  $m_2 = \beta_1 S - h\beta_2 I_{BD} - (\gamma + \theta_1 + \omega + \mu + \mu_1)$  and  $m_3 = \beta_2 S + h\beta_2 I_B - (\theta_2 + \rho + \mu + \mu_2)$ .

For the disease-free equilibrium the Jacobian at  $F_0$  is

$$J(F_0) = \begin{pmatrix} -\mu & -\beta_1 S^0 & -(\beta_1 + \beta_2)S^0 & 0 & 0 & 0 \\ 0 & \beta_1 S^0 - p_1 & 0 & 0 & 0 & 0 \\ 0 & 0 & \beta_2 S^0 - p_2 & 0 & 0 & 0 \\ 0 & \theta_1 & \theta_2 & -(\alpha + \tau + \mu) & 0 & 0 \\ 0 & \omega & \rho & \tau & -(\sigma + \mu) & 0 \\ 0 & \gamma & 0 & \alpha & \sigma & -\mu \end{pmatrix}.$$

The eigenvalue of the Jacobian matrix can be determine by solving,  $|J(F_0) - \lambda I| = 0$ .

$\lambda_1 = -\mu$ ,  $\lambda_4 = -(\alpha + \tau + \mu)$ ,  $\lambda_5 = -(\sigma + \mu)$ ,  $\lambda_6 = -\mu$ .

If  $R_0 < 1$  then  $R_{0B} < 1$  and  $R_{0BD} < 1$ , so

$$\lambda_2 = \beta_1 S^0 - p_1 = p_1(R_{0B} - 1) < 0, \quad \text{when } R_{0B} < 1,$$

$$\lambda_3 = \beta_2 S^0 - p_2 = p_2(R_{0BD} - 1) < 0, \quad \text{when } R_{0BD} < 1.$$

Then all eigenvalues are negative, according to Routh–Hurwitz criteria [12], the disease-free equilibrium  $F_0$  is locally asymptotically stable when  $R_0 < 1$  [22, 13].  $\square$

**Theorem 6.2.** Consider system (1) with DFE  $F_0 = \left(\frac{\Lambda}{\mu}, 0, 0, 0, 0, 0\right)$ . Assume that all model parameters are positive and let  $\Omega$  be the positively invariant feasible region defined in Section 3.

Suppose that:

**(H1)** The subsystem obtained from system (1) by setting  $I_B = I_{BD} = 0$  admits a unique equilibrium

$$X_0 = \left(\frac{\Lambda}{\mu}, 0, 0, 0\right) \text{ which is globally asymptotically stable in } \Omega.$$

Then, if the basic reproduction number  $R_0$  (defined in Section 5) satisfies  $R_0 < 1$ , the DFE  $F_0$  is globally asymptotically stable in  $\Omega$ .

*Proof.* We follow here the method of Castillo-Chavez global stability [10] and decompose the state variables into uninfected and infected classes. Let

$$X = (S, T, L, R), \quad Z = (I_B, I_{BD}).$$

Then system (1) can be written in the form  $\dot{X} = F(X, Z)$ ,  $\dot{Z} = G(X, Z)$ , where  $G(X, 0) = 0$  for all  $X \in \Omega$ .

**Verification of (H1).** Setting  $Z = 0$  reduces the system to

$$\begin{aligned}\dot{S} &= \Lambda - \mu S, \\ \dot{T} &= -(\alpha + \tau + \mu)T, \\ \dot{L} &= -(\sigma + \mu)L, \\ \dot{R} &= -\mu R.\end{aligned}$$

This linear autonomous system admits the unique equilibrium  $X_0 = \left(\frac{\Lambda}{\mu}, 0, 0, 0\right)$ , which is globally asymptotically stable in  $\Omega$ . Hence condition (H1) holds.

**Stability of the infected subsystem:** From the definition of  $R_0$  in Section 5, we know that  $R_0 = \rho(FV^{-1})$ , where  $F$  and  $V$  are the transmission and transition matrices of the infected subsystem evaluated at  $F_0$ .

If  $R_0 < 1$ , then all eigenvalues of the matrix  $F - V$  have negative real parts. Since  $F - V$  is a Metzler matrix, the linear system

$$\dot{Z} = (F - V)Z$$

is globally asymptotically stable at  $Z = 0$ .

Moreover, the nonlinear terms in the infected subsystem are nonpositive, so that

$$\dot{Z} \leq (F - V)Z.$$

By the comparison principle for cooperative systems,  $\lim_{t \rightarrow \infty} Z(t) = 0$ , that is,

$$\lim_{t \rightarrow \infty} I_B(t) = 0, \quad \lim_{t \rightarrow \infty} I_{BD}(t) = 0, \quad \text{whenever } R_0 < 1.$$

Since condition (H1) is satisfied and the infected subsystem converges to zero whenever  $R_0 < 1$ , all the hypotheses of the Castillo–Chávez and Song theorem [10] are fulfilled. Thus, the disease-free equilibrium  $F_0$  is globally asymptotically stable in  $\Omega$  whenever  $R_0 < 1$ .  $\square$

In the following section we will discuss the local stability of endemic equilibrium.

## 7. Local and Global Stability of the Endemic Equilibrium

In this section, we have discussed the local and global stability of the endemic equilibrium point  $F^*$  of model (1). In section 7.1 we shall discuss the Local Stability of the Endemic Equilibrium.

### 7.1. Local Stability of the Endemic Equilibrium

The local stability of the endemic equilibrium is established indirectly through a bifurcation analysis at the disease-free equilibrium using the center manifold theory of Castillo–Chavez and Song (2004) [10].

**Theorem 7.1** (Castillo-Chavez and Song (2004)). *Consider the epidemiological model  $\frac{dx}{dt} = f(x, \beta_1)$ ,  $x = (S, I_B, I_{BD}, T, L, R)^T$ , where  $f \in C^2(\mathbb{R}^6 \times \mathbb{R})$  and  $\beta_1$  is the bifurcation parameter. Let  $F_0$  be the disease-free equilibrium of the system, and let  $J = D_x f(F_0, \beta_1^*)$*

*be the Jacobian matrix of the system evaluated at  $F_0$ , where  $\beta_1 = \beta_1^*$  corresponds to  $R_{0B} = 1$ .*

*Assume that the following conditions hold:*

1. *The Jacobian matrix  $J$  has a simple zero eigenvalue, and all other eigenvalues have negative real parts.*

2. There exist right and left eigenvectors  $w$  and  $v$  of  $J$  associated with the zero eigenvalue such that

$$Jw = 0, \quad v^T J = 0,$$

with normalization  $v \cdot w = 1$ , where  $w$  is nonnegative.

Let  $f_k(x, \beta_1)$  denote the  $k$ -th component of  $f(x, \beta_1)$ . Define the bifurcation coefficients

$$\phi_1 = \sum_{k,i,j} v_k w_i w_j \frac{\partial^2 f_k(E_0, \beta_1^*)}{\partial x_i \partial x_j}, \quad \phi_2 = \sum_{k,i} v_k w_i \frac{\partial^2 f_k(E_0, \beta_1^*)}{\partial x_i \partial \beta_1}.$$

Then the following results hold:

1. If  $\phi_1 < 0$  and  $\phi_2 > 0$ , the disease-free equilibrium  $E_0$  undergoes a forward (supercritical) bifurcation at  $R_{0B} = 1$ . Consequently, a unique positive endemic equilibrium exists for  $R_{0B} > 1$ , and it is locally asymptotically stable.
2. If  $\phi_1 > 0$  and  $\phi_2 > 0$ , the system undergoes a backward (subcritical) bifurcation at  $R_{0B} = 1$ , and a locally asymptotically stable endemic equilibrium may exist even when  $R_{0B} < 1$ .

## 7.2. Bifurcation Analysis

To investigate the local dynamics of the model near DFE and, in specific, to characterize the emergence and local stability of an endemic equilibrium, we apply the center manifold method developed by Castillo-Chavez and Song [10]. The local dynamics near the Disease-Free Equilibrium can be characterized via the center manifold theory [16], reducing the system to the center manifold related with the zero eigenvalue. The bifurcation coefficients  $a$  and  $b$  then conclude the type of bifurcation and local stability of the endemic equilibrium. Our investigation is carried out in a neighborhood of the critical transmission rate  $\beta_1 = \beta_1^*$ , corresponding to the threshold condition  $R_0 = 1$ . At the mentioned critical value, the disease free equilibrium loses hyperbolicity, and the system may admit a branch of endemic equilibria. By explicitly calculating the right and left eigenvectors associated with the zero eigenvalue and computing the relevant bifurcation coefficients, we decide whether an endemic equilibrium bifurcates from the disease-free equilibrium and establish its local asymptotic stability for transmission rates exceeding the threshold  $\beta_1^*$ .

We consider the system 1, let the disease-free equilibrium be  $F_0$  and choose  $\phi = \beta_1$  as the bifurcation parameter.

### Computation Right and left eigenvector $w$ :

At  $R_{0B} = 1$ , the Jacobian  $J(F_0; \beta_1^*)$  has a simple zero eigenvalue. Let right eigenvector  $w = (w_1, w_2, w_3)^T$  correspond to the zero eigenvalue of the Jacobian restricted to  $(S, I_B, I_{BD})$ . Then

$$J(F_0)w = 0 \quad \implies \quad \begin{cases} -\mu w_1 - \beta_1^* S_0 w_2 - (\beta_1^* + \beta_2) S_0 w_3 = 0, \\ \beta_1^* S_0 w_3 = 0, \\ 0 = 0. \end{cases}$$

From the second equation, we get  $w_3 = 0$ .

Substituting  $w_3 = 0$  into the first equation gives  $w_1 = -\frac{\beta_1^* S_0}{\mu} w_2$ .

Thus, the right eigenvector is

$$w = \left( -\frac{\beta_1^* S_0}{\mu} w_2, w_2, 0 \right), \quad w_2 > 0.$$

Let  $v = (v_1, v_2, v_3)$  the left eigenvector corresponding to the zero eigenvalue. Solve

$$v^T J(F_0) = 0 \implies \begin{cases} -\mu v_1 = 0 & \Rightarrow v_1 = 0, \\ -(\beta_1^* + \beta_2) S_0 v_1 + \beta_1^* S_0 v_2 + (\beta_2 S_0 - p_2) v_3 = 0. \end{cases}$$

Plugging  $v_1 = 0$  gives  $v_3 = -\frac{\beta_1^* S_0}{p_2 - \beta_2 S_0} v_2$ ,  $v_2 > 0$ .  
Hence the left eigenvector is

$$v = \left( 0, v_2, -\frac{\beta_1^* S_0}{p_2 - \beta_2 S_0} v_2 \right), \quad v_2 > 0$$

For the full system, only infected compartments contribute to new infections, so

$$v_1 = v_4 = v_5 = v_6 = 0.$$

Similarly, the right eigenvector satisfies  $w_2, w_3 > 0$ ,  $w_1 < 0$ .

### **Computation of Nonzero second derivatives**

The nonlinear terms in the model are

$$f_2 = \beta_1 S(I_B + I_{BD}) - h\beta_2 I_B I_{BD} - p_1 I_B, \quad f_3 = \beta_2 S I_{BD} + h\beta_2 I_B I_{BD} - p_2 I_{BD}.$$

The nonzero second derivatives at  $F_0$  are

$$\frac{\partial^2 f_2}{\partial S \partial I_B} = \beta_1, \quad \frac{\partial^2 f_2}{\partial S \partial I_{BD}} = \beta_1, \quad \frac{\partial^2 f_2}{\partial I_B \partial I_{BD}} = -h\beta_2, \quad \frac{\partial^2 f_3}{\partial S \partial I_{BD}} = \beta_2, \quad \frac{\partial^2 f_3}{\partial I_B \partial I_{BD}} = h\beta_2.$$

All other second derivatives are zero.

### **Computation of $\phi_1$ :**

By definition,  $\phi_1 = \sum_{k,i,j} v_k w_i w_j \frac{\partial^2 f_k(E_0, 0)}{\partial x_i \partial x_j}$ .

Only  $f_2$  and  $f_3$  contribute:

$$\begin{aligned} \phi_1 &= v_2 (w_1 w_2 \beta_1 + w_1 w_3 \beta_1 - w_2 w_3 h \beta_2) + v_3 (w_1 w_3 \beta_2 + w_2 w_3 h \beta_2) \\ &= v_2 (\beta_1 w_1 w_2 + \beta_1 w_1 w_3 - h \beta_2 w_2 w_3) + v_3 (\beta_2 w_1 w_3 + h \beta_2 w_2 w_3). \end{aligned}$$

Since  $w_1 < 0$  and  $w_2, w_3, v_2, v_3 > 0$ , we have  $\phi_1 < 0$ .

### **Computation of $\phi_2$ :**

By definition,  $\phi_2 = \sum_{k,i} v_k w_i \frac{\partial^2 f_k(F_0, 0)}{\partial x_i \partial \beta_1}$ .

Only  $f_2$  depends on  $\beta_1$ . At  $F_0$ ,

$$\frac{\partial^2 f_2}{\partial I_B \partial \beta_1} = S^0, \quad \frac{\partial^2 f_2}{\partial I_{BD} \partial \beta_1} = S^0, \quad \frac{\partial^2 f_2}{\partial S \partial \beta_1} = 0.$$

Thus,  $\phi_2 = v_2(w_2S^0 + w_3S^0) = v_2S^0(w_2 + w_3) > 0$ .

Since  $\phi_1 < 0$  and  $\phi_2 > 0$ , Hence, by Theorem [10], the disease-free equilibrium  $F_0$  loses stability as  $R_{0B}$  crosses unity from below and a unique positive endemic equilibrium emerges. Therefore, the model undergoes a forward (supercritical) bifurcation at  $R_{0B} = 1$ , and the endemic equilibrium is locally asymptotically stable for  $R_{0B} > 1$ , and theorem 7.1 proved.

### 7.3. Global Stability at the Endemic Equilibrium

In this section, we investigate the global asymptotic stability of the endemic equilibrium point  $F^*$  of model (1).

**Theorem 7.2.** *For model (1), if  $R_0 > 1$ , then the endemic equilibrium point  $F^*$  is globally asymptotically stable in the feasible region  $\Omega$ .*

*Proof.* To establish the global stability of the endemic equilibrium  $F^*$ , we define the Lyapunov function  $G$  [25] as

$$G = \frac{1}{2} [(S - S^*) + (I_B - I_B^*) + (I_{BD} - I_{BD}^*) + (T - T^*) + (L - L^*) + (R - R^*)]^2. \quad (6)$$

Clearly,  $G \geq 0$  for all  $(S, I_B, I_{BD}, T, L, R) \in \Omega$ , and

$$G = 0 \quad \text{if and only if} \quad (S, I_B, I_{BD}, T, L, R) = (S^*, I_B^*, I_{BD}^*, T^*, L^*, R^*).$$

Hence,  $G$  is positive definite with respect to the endemic equilibrium  $F^*$ . Since  $N(t) = S(t) + I_B(t) + I_{BD}(t) + T(t) + L(t) + R(t)$ , and  $N^*(t) = S^*(t) + I_B^*(t) + I_{BD}^*(t) + T^*(t) + L^*(t) + R^*(t)$ ,

Differentiating  $G$  along the trajectories of system (1) yields

$$\frac{dG}{dt} = (N - N^*) \frac{dN}{dt}.$$

Summing all the equations of system (1), we obtain

$$\frac{dN}{dt} = \Lambda - \mu N - \mu_1 I_B - \mu_2 I_{BD} \leq \Lambda - \mu N.$$

Therefore,

$$\frac{dG}{dt} \leq (N - N^*)(\Lambda - \mu N) = -\mu \left( N - \frac{\Lambda}{\mu} \right)^2 \leq 0.$$

Thus,  $\frac{dG}{dt}$  is negative semi-definite. Moreover,  $\frac{dG}{dt} = 0$  if and only if  $N = N^*$ . The largest invariant set contained in  $\{(S, I_B, I_{BD}, T, L, R) \in \Omega : \frac{dG}{dt} = 0\}$  is the singleton set  $\{F^*\}$ . Hence, by LaSalle's invariance principle [26], every solution of model (1) with initial conditions in  $\Omega$  approaches the endemic equilibrium point  $F^*$  as  $t \rightarrow \infty$ . Consequently, the endemic equilibrium  $F^*$  is globally asymptotically stable in  $\Omega$  whenever  $R_0 > 1$  [13].  $\square$

In the next section, we examine the sensitivity analysis of the model parameters.

## 8. Sensitivity Analysis

In this section, we calculate the sensitivity of the basic reproduction number  $R_0$  with respect to the model parameters, as understanding this sensitivity is decisive for recognizing the factors that most

powerfully influence the transmission and control of Hepatitis B Virus (HBV) [23]. Sensitivity study classifies the parameters that utilize the maximum influence on disease dynamics [1], thereby serving in the system of extra effective intervention strategies. As a consequence, we communicate about a sensitivity analysis of the vital parameters in the HBV model (1) to predict its effect on simple  $R_0$ . The standardized forward sensitivity indices are calculated following the approach offered by Chitnis et al. [11], wherever the sensitivity index of  $R_0$  with respect to a parameter  $r$  is defined as:

$$Z_r^{R_0} = \frac{\partial R_0}{\partial r} \times \frac{r}{R_0}, \quad (7)$$

$$\text{where } r \in \{\Lambda, \beta_1, \beta_2, \mu, \gamma, \omega, \theta_1, \mu_1, \rho, \theta_2, \mu_2\}. \quad (8)$$

Here we evaluate 7 for each parameter in 8

$$\begin{aligned} Z_{\Lambda}^{R_0} &= 1 & Z_{\beta_1}^{R_0} &= \frac{\beta_1 p_2}{p_2 \beta_1 + \beta_2 p_1} \\ Z_{\beta_2}^{R_0} &= \frac{\beta_2 p_1}{p_1 \beta_2 + \beta_1 p_2} & Z_{\mu}^{R_0} &= - \left[ \frac{\mu}{R_0} \left( \frac{\Lambda \beta_1 p_1 + \Lambda \beta_1 \mu}{\mu^2 p_1^2} + \frac{\Lambda \beta_2 p_2 + \Lambda \beta_2 \mu}{\mu^2 p_2^2} \right) \right] \\ Z_{\gamma}^{R_0} &= - \frac{\gamma}{p_1} \cdot \frac{\Lambda \beta_1}{R_0 \mu} & Z_{\omega}^{R_0} &= - \frac{\omega}{p_1} \cdot \frac{\Lambda \beta_1}{R_0 \mu} \\ Z_{\theta_1}^{R_0} &= - \frac{\theta_1}{p_1} \cdot \frac{\Lambda \beta_1}{R_0 \mu} & Z_{\mu_1}^{R_0} &= - \frac{\mu_1}{p_1} \cdot \frac{\Lambda \beta_1}{R_0 \mu} \\ Z_{\rho}^{R_0} &= - \frac{\rho}{p_2} \cdot \frac{\Lambda \beta_2}{R_0 \mu} & Z_{\theta_2}^{R_0} &= - \frac{\theta_2}{p_2} \cdot \frac{\Lambda \beta_2}{R_0 \mu} \\ Z_{\mu_2}^{R_0} &= - \frac{\mu_2}{p_2} \cdot \frac{\Lambda \beta_2}{R_0 \mu}. \end{aligned}$$

To certify our theoretical findings, we made numerical simulations using the 4th-order Runge-Kutta method. The parameter values employed in the simulations are given in Table 1, primarily drawn from available literature, containing reports by the World Health Organization and other epidemiological studies. The PRCCs corresponding to these parameters in relation to  $R_0$  are publicized in Figure 2. As shown in Figure 4 that our conclusions identify that the parameters  $\Lambda$ ,  $\beta_1$ , and  $\beta_2$  are positively correlated with  $R_0$ , while  $\gamma$ ,  $\mu$ ,  $\mu_1$ ,  $\mu_2$ ,  $\theta_1$ ,  $\theta_2$ ,  $\omega$ , and  $\rho$  display a negative correlation. Besides,  $\beta_1$ ,  $\beta_2$ ,  $\theta_1$ , and  $\theta_2$  are the most sensitive parameters with respect to  $R_0$ . Therefore, dropping  $\beta_1$  and  $\beta_2$ , while growing  $\theta_1$  and  $\theta_2$ , can effectively donate to controlling HBV and HDV co-infection.

Figure 4: The graph displays the sensitivity of  $R_0$  with effect of different parameters

In the following section we will present numerical scheme of the model.

## 9. Numerical Scheme

This unit supports the numerical examination of the epidemic model (1) with RK4 method and NSFD system instigated in MATLAB. Various parameters with numerical values are given in Table 1, the model consist of various parameters with definite numerical values. As RK4 and NSFD techniques are hired to simulate the model dynamics, constructing numerical results and graphical outputs that elucidate the progressive evolution of the sections and important patterns in HBV–HDV transmission. In addition, the simulations appraised the effects of changing initial conditions and parameter values, providing insights into the model's sensitivity and fundamental constancy.

### 9.1. Runge-Kutta 4th Order Method for the Model

We denote the variables at time  $t_n$  as  $S_n, I_{Bn}, I_{BDn}, T_n, L_n, R_n$ , and use step size  $h$ . The RK4 steps are defined as follows.

#### Step 1: Compute $k_1$

$$\begin{aligned} k_{1S} &= \Lambda - \beta_1 S_n (I_{Bn} + I_{BDn}) - \beta_2 S_n I_{BDn} - \mu S_n, \\ k_{1I_B} &= \beta_1 S_n (I_{Bn} + I_{BDn}) - h\beta_2 I_{Bn} I_{BDn} - (\gamma + \theta_1 + \omega + \mu + \mu_1) I_{Bn}, \\ k_{1I_{BD}} &= \beta_2 S_n I_{BDn} + h\beta_2 I_{Bn} I_{BDn} - (\theta_2 + \rho + \mu + \mu_2) I_{BDn}, \\ k_{1T} &= \theta_1 I_{Bn} + \theta_2 I_{BDn} - (\alpha + \tau + \mu) T_n, \\ k_{1L} &= \rho I_{BDn} + \tau T_n + \omega I_{Bn} - (\sigma + \mu) L_n, \\ k_{1R} &= \gamma I_{Bn} + \alpha T_n + \sigma L_n - \mu R_n. \end{aligned}$$

#### Step 2: Compute $k_2$

$$\begin{aligned} k_{2S} &= \Lambda - \beta_1 (S_n + \frac{h}{2} k_{1S}) (I_{Bn} + \frac{h}{2} k_{1I_B} + I_{BDn} + \frac{h}{2} k_{1I_{BD}}) \\ &\quad - \beta_2 (S_n + \frac{h}{2} k_{1S}) (I_{BDn} + \frac{h}{2} k_{1I_{BD}}) - \mu (S_n + \frac{h}{2} k_{1S}), \\ k_{2I_B} &= \beta_1 (S_n + \frac{h}{2} k_{1S}) (I_{Bn} + \frac{h}{2} k_{1I_B} + I_{BDn} + \frac{h}{2} k_{1I_{BD}}) \\ &\quad - h\beta_2 (I_{Bn} + \frac{h}{2} k_{1I_B}) (I_{BDn} + \frac{h}{2} k_{1I_{BD}}) \\ &\quad - (\gamma + \theta_1 + \omega + \mu + \mu_1) (I_{Bn} + \frac{h}{2} k_{1I_B}), \\ k_{2I_{BD}} &= \beta_2 (S_n + \frac{h}{2} k_{1S}) (I_{BDn} + \frac{h}{2} k_{1I_{BD}}) + h\beta_2 (I_{Bn} + \frac{h}{2} k_{1I_B}) (I_{BDn} + \frac{h}{2} k_{1I_{BD}}) \\ &\quad - (\theta_2 + \rho + \mu + \mu_2) (I_{BDn} + \frac{h}{2} k_{1I_{BD}}), \\ k_{2T} &= \theta_1 (I_{Bn} + \frac{h}{2} k_{1I_B}) + \theta_2 (I_{BDn} + \frac{h}{2} k_{1I_{BD}}) - (\alpha + \tau + \mu) (T_n + \frac{h}{2} k_{1T}), \\ k_{2L} &= \rho (I_{BDn} + \frac{h}{2} k_{1I_{BD}}) + \tau (T_n + \frac{h}{2} k_{1T}) + \omega (I_{Bn} + \frac{h}{2} k_{1I_B}) \\ &\quad - (\sigma + \mu) (L_n + \frac{h}{2} k_{1L}), \\ k_{2R} &= \gamma (I_{Bn} + \frac{h}{2} k_{1I_B}) + \alpha (T_n + \frac{h}{2} k_{1T}) + \sigma (L_n + \frac{h}{2} k_{1L}) - \mu (R_n + \frac{h}{2} k_{1R}). \end{aligned}$$

**Step 3: Compute  $k_3$**

$$\begin{aligned}
k_{3S} &= \Lambda - \beta_1(S_n + \frac{h}{2}k_{2S})(I_{Bn} + \frac{h}{2}k_{2I_B} + I_{BDn} + \frac{h}{2}k_{2I_{BD}}) \\
&\quad - \beta_2(S_n + \frac{h}{2}k_{2S})(I_{BDn} + \frac{h}{2}k_{2I_{BD}}) - \mu(S_n + \frac{h}{2}k_{2S}), \\
k_{3I_B} &= \beta_1(S_n + \frac{h}{2}k_{2S})(I_{Bn} + \frac{h}{2}k_{2I_B} + I_{BDn} + \frac{h}{2}k_{2I_{BD}}) \\
&\quad - h\beta_2(I_{Bn} + \frac{h}{2}k_{2I_B})(I_{BDn} + \frac{h}{2}k_{2I_{BD}}) \\
&\quad - (\gamma + \theta_1 + \omega + \mu + \mu_1)(I_{Bn} + \frac{h}{2}k_{2I_B}), \\
k_{3I_{BD}} &= \beta_2(S_n + \frac{h}{2}k_{2S})(I_{BDn} + \frac{h}{2}k_{2I_{BD}}) + h\beta_2(I_{Bn} + \frac{h}{2}k_{2I_B})(I_{BDn} + \frac{h}{2}k_{2I_{BD}}) \\
&\quad - (\theta_2 + \rho + \mu + \mu_2)(I_{BDn} + \frac{h}{2}k_{2I_{BD}}), \\
k_{3T} &= \theta_1(I_{Bn} + \frac{h}{2}k_{2I_B}) + \theta_2(I_{BDn} + \frac{h}{2}k_{2I_{BD}}) - (\alpha + \tau + \mu)(T_n + \frac{h}{2}k_{2T}), \\
k_{3L} &= \rho(I_{BDn} + \frac{h}{2}k_{2I_{BD}}) + \tau(T_n + \frac{h}{2}k_{2T}) + \omega(I_{Bn} + \frac{h}{2}k_{2I_B}) \\
&\quad - (\sigma + \mu)(L_n + \frac{h}{2}k_{2L}), \\
k_{3R} &= \gamma(I_{Bn} + \frac{h}{2}k_{2I_B}) + \alpha(T_n + \frac{h}{2}k_{2T}) + \sigma(L_n + \frac{h}{2}k_{2L}) - \mu(R_n + \frac{h}{2}k_{2R}).
\end{aligned}$$

**Step 4: Compute  $k_4$**

$$\begin{aligned}
k_{4S} &= \Lambda - \beta_1(S_n + hk_{3S})(I_{Bn} + hk_{3I_B} + I_{BDn} + hk_{3I_{BD}}) \\
&\quad - \beta_2(S_n + hk_{3S})(I_{BDn} + hk_{3I_{BD}}) - \mu(S_n + hk_{3S}), \\
k_{4I_B} &= \beta_1(S_n + hk_{3S})(I_{Bn} + hk_{3I_B} + I_{BDn} + hk_{3I_{BD}}) \\
&\quad - h\beta_2(I_{Bn} + hk_{3I_B})(I_{BDn} + hk_{3I_{BD}}) \\
&\quad - (\gamma + \theta_1 + \omega + \mu + \mu_1)(I_{Bn} + hk_{3I_B}), \\
k_{4I_{BD}} &= \beta_2(S_n + hk_{3S})(I_{BDn} + hk_{3I_{BD}}) + h\beta_2(I_{Bn} + hk_{3I_B})(I_{BDn} + hk_{3I_{BD}}) \\
&\quad - (\theta_2 + \rho + \mu + \mu_2)(I_{BDn} + hk_{3I_{BD}}), \\
k_{4T} &= \theta_1(I_{Bn} + hk_{3I_B}) + \theta_2(I_{BDn} + hk_{3I_{BD}}) - (\alpha + \tau + \mu)(T_n + hk_{3T}), \\
k_{4L} &= \rho(I_{BDn} + hk_{3I_{BD}}) + \tau(T_n + hk_{3T}) + \omega(I_{Bn} + hk_{3I_B}) \\
&\quad - (\sigma + \mu)(L_n + hk_{3L}), \\
k_{4R} &= \gamma(I_{Bn} + hk_{3I_B}) + \alpha(T_n + hk_{3T}) + \sigma(L_n + hk_{3L}) - \mu(R_n + hk_{3R}).
\end{aligned}$$

**Final Update Equations**

$$\begin{aligned}
S_{n+1} &= S_n + \frac{h}{6}(k_{1S} + 2k_{2S} + 2k_{3S} + k_{4S}), \\
I_{B,n+1} &= I_{Bn} + \frac{h}{6}(k_{1I_B} + 2k_{2I_B} + 2k_{3I_B} + k_{4I_B}), \\
I_{BD,n+1} &= I_{BDn} + \frac{h}{6}(k_{1I_{BD}} + 2k_{2I_{BD}} + 2k_{3I_{BD}} + k_{4I_{BD}}), \\
T_{n+1} &= T_n + \frac{h}{6}(k_{1T} + 2k_{2T} + 2k_{3T} + k_{4T}), \\
L_{n+1} &= L_n + \frac{h}{6}(k_{1L} + 2k_{2L} + 2k_{3L} + k_{4L}), \\
R_{n+1} &= R_n + \frac{h}{6}(k_{1R} + 2k_{2R} + 2k_{3R} + k_{4R}).
\end{aligned}$$

## 9.2. NSFD Scheme Calculation for the Proposed Model Equations

The original system of differential equations is given by:

$$\begin{aligned}\frac{dS}{dt} &= \Lambda - \beta_1 S(I_B + I_{BD}) - \beta_2 S I_{BD} - \mu S, \\ \frac{dI_B}{dt} &= \beta_1 S(I_B + I_{BD}) - h\beta_2 I_B I_{BD} - (\gamma + \theta_1 + \omega + \mu + \mu_1) I_B, \\ \frac{dI_{BD}}{dt} &= \beta_2 S I_{BD} + h\beta_2 I_B I_{BD} - (\theta_2 + \rho + \mu + \mu_2) I_{BD}, \\ \frac{dT}{dt} &= \theta_1 I_B + \theta_2 I_{BD} - (\alpha + \tau + \mu) T, \\ \frac{dL}{dt} &= \rho I_{BD} + \tau T + \omega I_B - (\sigma + \mu) L, \\ \frac{dR}{dt} &= \gamma I_B + \alpha T + \sigma L - \mu R.\end{aligned}$$

**Discretization of Time:** Let  $t_n = n\Delta t$ , where  $\Delta t$  is the time step. We approximate derivatives using forward differences:

$$\frac{dX}{dt} \approx \frac{X_{n+1} - X_n}{\Delta t}.$$

### NSFD Scheme

We incorporate a nonstandard denominator for the nonlinear terms to preserve the dynamical properties of the system. Below is the NSFD formulation for each equation.

$$\begin{aligned}\frac{S_{n+1} - S_n}{\Delta t} &= \Lambda - \frac{\beta_1 S_n (I_{B_n} + I_{BD_n})}{1 + hS_n} - \frac{\beta_2 S_n I_{BD_n}}{1 + hS_n} - \mu S_n \\ \Rightarrow S_{n+1} &= S_n + \Delta t \left( \Lambda - \frac{\beta_1 S_n (I_{B_n} + I_{BD_n}) + \beta_2 S_n I_{BD_n}}{1 + hS_n} - \mu S_n \right), \\ \frac{I_{B_{n+1}} - I_{B_n}}{\Delta t} &= \frac{\beta_1 S_n (I_{B_n} + I_{BD_n})}{1 + hS_n} - h\beta_2 I_{B_n} I_{BD_n} - (\gamma + \theta_1 + \omega + \mu + \mu_1) I_{B_n} \\ \Rightarrow I_{B_{n+1}} &= I_{B_n} + \Delta t \left( \frac{\beta_1 S_n (I_{B_n} + I_{BD_n})}{1 + hS_n} - h\beta_2 I_{B_n} I_{BD_n} - (\gamma + \theta_1 + \omega + \mu + \mu_1) I_{B_n} \right), \\ \frac{I_{BD_{n+1}} - I_{BD_n}}{\Delta t} &= \frac{\beta_2 S_n I_{BD_n}}{1 + hS_n} + h\beta_2 I_{B_n} I_{BD_n} - (\theta_2 + \rho + \mu + \mu_2) I_{BD_n} \\ \Rightarrow I_{BD_{n+1}} &= I_{BD_n} + \Delta t \left( \frac{\beta_2 S_n I_{BD_n}}{1 + hS_n} + h\beta_2 I_{B_n} I_{BD_n} - (\theta_2 + \rho + \mu + \mu_2) I_{BD_n} \right), \\ \frac{T_{n+1} - T_n}{\Delta t} &= \theta_1 I_{B_n} + \theta_2 I_{BD_n} - (\alpha + \tau + \mu) T_n \\ \Rightarrow T_{n+1} &= T_n + \Delta t (\theta_1 I_{B_n} + \theta_2 I_{BD_n} - (\alpha + \tau + \mu) T_n).\end{aligned}$$

$$\begin{aligned}
\frac{L_{n+1} - L_n}{\Delta t} &= \rho I_{BD_n} + \tau T_n + \omega I_{B_n} - (\sigma + \mu)L_n \\
&\Rightarrow L_{n+1} = L_n + \Delta t (\rho I_{BD_n} + \tau T_n + \omega I_{B_n} - (\sigma + \mu)L_n), \\
\frac{R_{n+1} - R_n}{\Delta t} &= \gamma I_{B_n} + \alpha T_n + \sigma L_n - \mu R_n \\
&\Rightarrow R_{n+1} = R_n + \Delta t (\gamma I_{B_n} + \alpha T_n + \sigma L_n - \mu R_n).
\end{aligned}$$

### Summary of NSFD Scheme

$$\begin{aligned}
S_{n+1} &= S_n + \Delta t \left( \Lambda - \frac{\beta_1 S_n (I_{B_n} + I_{BD_n}) + \beta_2 S_n I_{BD_n}}{1 + h S_n} - \mu S_n \right), \\
I_{B_{n+1}} &= I_{B_n} + \Delta t \left( \frac{\beta_1 S_n (I_{B_n} + I_{BD_n})}{1 + h S_n} - h \beta_2 I_{B_n} I_{BD_n} - (\gamma + \theta_1 + \omega + \mu + \mu_1) I_{B_n} \right), \\
I_{BD_{n+1}} &= I_{BD_n} + \Delta t \left( \frac{\beta_2 S_n I_{BD_n}}{1 + h S_n} + h \beta_2 I_{B_n} I_{BD_n} - (\theta_2 + \rho + \mu + \mu_2) I_{BD_n} \right), \\
T_{n+1} &= T_n + \Delta t (\theta_1 I_{B_n} + \theta_2 I_{BD_n} - (\alpha + \tau + \mu) T_n), \\
L_{n+1} &= L_n + \Delta t (\rho I_{BD_n} + \tau T_n + \omega I_{B_n} - (\sigma + \mu) L_n), \\
R_{n+1} &= R_n + \Delta t (\gamma I_{B_n} + \alpha T_n + \sigma L_n - \mu R_n).
\end{aligned}$$

## 10. Numerical Simulation

The stability analysis of the HBV/HDV co-infection model focuses on both the DFE and the EE. By varying main epidemiological and clinical parameters in system (1), the impact on every class can be inspected through the reproduction number  $R_0$ , which measures the transmission potential of the infection. As shown in Figure 8a, when  $R_0 < 1$ , all infection-related classes including HBV-only infected ( $I_B$ ), co-infected ( $I_{BD}$ ), treatment ( $T$ ), and liver transplant ( $L$ ) decline slowly and approach zero. At the same time, the susceptible class ( $S$ ) rises and stabilizes at a high level, while the recovered population ( $R$ ) increases initially and then slowly decays as the system settles. This conduct reflects the convergence of the model towards a stable DFE, confirming that the infection cannot continue in the long run when each infected individual creates less than one secondary case on average.

In contrast, Figure 8c validates the scenario when  $R_0 > 1$ . In this instance, the infection-linked compartments rise primarily and then stabilize at positive levels, which signifying the continual presence of the sickness in the human population. The susceptible class falls from its initial value and then stabilizes at a lower equilibrium point, however the recovered people rises during the primary phase and then levels off at a high value. This consideration identifies a stable EE, where the infection exists at controlled, however non-zero levels even with the execution of treatment and liver transplant interfering. Overall these judgments shows an important role of the basic reproduction number,  $R_0$ , in affecting the long-term deductions of the disease. The disease-free equilibrium is attained after  $R_0 < 1$ , establishing the eventual elimination of HBV/HDV co-infection. Once  $R_0 > 1$ , the endemic situation is achieved in the population. Figures 5 expresses the effect of the transmission rate  $\beta_1$  on the dynamics of uncountable residents in the HBV model, simulated with the RK4 outline. For the susceptible, greater  $\beta_1$  causes an earlier decline and lead to lower minimum levels, but smaller values approval  $S(t)$  to stabilize at relatively higher levels. In similar, for the  $I_B(t)$  and  $I_{BD}(t)$  classes, more values of  $\beta_1$  result in expanded infection phases, but reduced values speed up their decay. These explanations stress the crucial importance of tumbling transmission rates to effectively control both infections.

In similar way the liver transplant  $L(t)$  and treated  $T(t)$  drop speedily across all  $\beta_1$  values and stabilize at very low levels with least difference, which of course indicating narrow sensitivity to variations in the transmission rate. The recovered residents  $R(t)$  growing initially to a peak and then steadily decreases; higher  $\beta_1$  values lead to more sustained recovery levels, while lesser values product in quicker declines. In general, it is important to lower  $\beta_1$  for decreasing both infections rates and attaining more satisfactory results for classes.

In Figure 6 the comparison between RK4 and NSFD displays that the solutions of both methods are very adjacent and almost overlap for all compartments. The trajectories of classes  $S(t)$ ,  $I_B(t)$ ,  $T(t)$ , and  $L(t)$  are closely identical, which indicates strong numerical agreement and stability. Only in the recovered class  $R(t)$  a very small change is detected in the transient phase, where the peak values vary slightly, but both approaches converge to the similar long-term behavior. The results produced with the NSFD system are consistent with RK4, maintaining the qualitative dynamics of the proposed model. Since initial conditions for all compartments are  $S_0 = 300$ ,  $I_{B0} = 80$ ,  $I_{BD0} = 80$ ,  $T_0 = 70$ ,  $L_0 = 70$ ,  $t_0 = 0$ ,  $t_f = 500$ ,  $\Delta t = 0.1$ . The parameter values hired in the numerical simulations, with their sources, are offered in Table. 1.

Table 1: Model Parameters, Values, and Sources

Parameters	Values	Source / Notes
$\Lambda$	4	Assumed
$\mu$	0.01	[39]
$\beta_1, \beta_2$	$3 \times 10^{-5}, 3 \times 10^{-5}$	[39]
$h$	0.1	Assumed
$\gamma$	0.001	[6]
$\theta_1$	0.01	[15]
$\omega$	0.001	[24]
$\mu_1, \mu_2$	0.0001, 0.0001	[3]
$\theta_2$	0.01	[15]
$\rho$	0.01	[24]
$\alpha$	0.1	[6]
$\tau$	0.01	[15]
$\sigma$	0.1	[24]

Since the phase portraits in Figures 7 irradiate the dynamic interactions amongst major classes of the HBV-HDV co-infection model. Figure 7a reveals the relationship between the ( $S$ ) and ( $I_B$ ) residents, where  $S$  falls as  $I_B$  rises before both touches equilibrium. A correlated improvement is noticed in Figure 7b between  $S$  and the co-infected ( $I_{BD}$ ), with co-infections developing as susceptibility drops, supervised by stabilization. Figure 7c unveils the connection between  $S$  and the liver transplant ( $L$ ), screening an initial growth in ( $L$ ) due to superior infection levels, followed by a reduction as recovery occurs. The opposite link between  $S$  and ( $R$ ), displayed in Figure 7d, shows that declining susceptibility associates with growing recovery till equilibrium is accessed. The communication between  $I_B$  and  $I_{BD}$  in Figure 7e displays initial growth in both due to joint transmission tracks, measured by decline by way of infection diminishes. Figure 7f calls how the treated residents grows with greater co-infection ranks and later descents, repeating effective interventions. In conclusion, Figure 7g highlights the linkage between  $T$  and  $L$ , where superior treatment shrinks transplant demand, and both compartments become stable over time. Finally, Figure 7h grants the interaction between  $L$  and  $R$ , revealing an inverse relationship in which recovery rises as the need for transplantation declines, representing successful long-term management and the system's convergence to a steady state

- (a) The time-varying quantity of susceptible entities ( $S$ )
- (b) The time-varying quantity of HBV infected entities ( $I_B$ )
- (c) The time-varying quantity of HBV-HDV Co-infected entities ( $I_{BD}$ )
- (d) The time-varying quantity Treated entities ( $T$ )
- (e) The time-varying quantity of liver transplanted entities ( $L$ )
- (f) The time-varying quantity of recovered entities ( $R$ )

Figure 5: The graphs indicates the effect of various values of parameter  $\beta = 0.00001, 0.00002, 0.00003, 0.00004, 0.00005$  varying with time on, (a) susceptible entities  $S$ . (b) The number of HBV infected entities ( $I_B$ ). (c) The number of HBV-HDV Co-infected entities ( $I_{BD}$ ). (d) The number of Treated entities ( $T$ ). (e) The number liver transplanted entities ( $L$ ). (f) The number of recovered entities ( $R$ ).

(a) Comparison of susceptibles  $S$  by Rk4 Method and NSFD Method

(b) Comparison of HBV infected  $I_B$  by Rk4 Method and NSFD Method

(c) Comparison of HBV-HDV infected  $I_{BD}$  by Rk4 and NSFD Method

(d) Comparison of Treated  $T$  by Rk4 Method and NSFD Method

(e) Comparison of Liver Transplanted  $L$  by Rk4 Method and NSFD Method

(f) Comparison of Recovered  $R$  by Rk4 Method and NSFD Method

Figure 6: The graphs indicate the comparison of the specified classes using the RK4 method and the NSFD method over time. (a) Number of Susceptible entities  $S$ . (b) Number of HBV infected entities  $I_B$ . (c) Number of HBV-HDV infected entities  $I_{BD}$ . (d) Number of Treated entities  $T$ . (e) Number of Liver Transplanted entities  $L$ . (f) Number of recovered entities  $R$ .

When RK4 and NSFD methods yield similar graphs (as in fig. 6), it can be observed as an ideal situation, but distinctions exist. While alike graphs from RK4 and NSFD can be realized as an ideal situation reflecting decent numerical performance, it is important to maintain a critical perspective.

- (a) Susceptible vs HBV-infected individuals
- (b) Susceptible vs HBV-HDV co-infected individuals
- (c) Susceptible vs Liver transplant candidates
- (d) Susceptible vs Recovered individuals
- (e) HBV-infected vs HBV-HDV co-infected individuals
- (f) HBV-HDV co-infected vs Treated individuals
- (g) Treated individuals vs Liver transplant candidates
- (h) Liver transplant candidates vs Recovered individuals

Figure 7: Phase portraits showing the dynamic relationships between different compartments in the HBV-HDV co-infection model: (a)  $S$  vs  $I_B$ ; (b)  $S$  vs  $I_{BD}$ ; (c)  $S$  vs  $L$ ; (d)  $S$  vs  $R$ ; (e)  $I_B$  vs  $I_{BD}$ ; (f)  $I_{BD}$  vs  $T$ ; (g)  $T$  vs  $L$ ; (h)  $L$  vs  $R$ .

Figure 8: The graphs in (a) and (b) shows the comparison of Disease-free equilibrium points by RK4 method and NsFD method respectively, while the graph in (c) shows the endemic equilibrium points of model.

## 11. Conclusion Remarks

In this article, we made and analyzed a deterministic model to explore the transmission propagation of HBV and HDV co-infection. The model emphasizes on direct transmission pathways and incorporates main epidemiological units, containing susceptible individuals, HBV-infected and HBV–HDV co-infected classes, treated patients, liver transplant recipients, and recovered entities. The basic reproduction number  $R_0$  was derived as a threshold needle of disease propagation. Critical results discovered that the disease-free equilibrium is locally and globally asymptotically stable after  $R_0 < 1$ , showing subsequent annihilation, though an endemic equilibrium survives for  $R_0 > 1$ , signifying perseverance of infection. Numerical simulations done in MATLAB set these theoretical findings and revealed the long-term performance of each compartment under fluctuating  $R_0$  values. The obtained results performed a big role of primary treatment coverage and liver transplantation as a lifesaving choice in disease related deaths. In brief, this script has developed the need for early cure of infected individuals, their clinical facility, and the healthcare facility for saving lives through liver transplant. The above-stated model (1) has been statistically tested with the help of Runge-Kutta and NsFD schemes, and therefore consistency in these statistical techniques has validated the stability of the developed model. Since the model (1) does not yield any result concerning vaccinations or environmental factors, it provides significant insight into the spreading and control of HBV-HDV co-infection in the human population without the support of any booster forces. With the inclusion of various parameters like immune response, older age group, and random events, the model can be extended, and corrections can be made based on real-world data for better accuracy in humanities. However, in reality, the findings from the above-discussed model have helped to give ways both theoretically and practically to tackle problems of coinfections of hepatitis B virus and hepatitis D virus.

### **Declarations:**

**Challenging benefits:** Authors believe that there is no benefit which can be regarded as a challenging one for them.

**Funding:** The development of this paper did not involve any financial help.

**Interaction between writers:** All authors have equally contributed to the preparation of this paper. They have examined and approved the final version of this manuscript.

**Data availability statement:** All the data used to perform the present research are included in the manuscript.

**Artificial intelligence tool statement:** Writers state that none of the Artificial Intelligence tools were used in the creation of the paper.

**Acknowledgements:** Not applicable.

All authors have read and approved the last version of this manuscript.

## References

- [1] I. Ahmad, F. Hussain, N. Mlaiki, N. Ali, Z. Ullah, A. A. Eid, and N. Fatima, “Stability and bifurcation analysis of an epidemic model for Ebola virus dynamics with control strategies,” *Fractals* (2025).
- [2] M. J. Alter, B. L. Evatt, H. S. Margolis, R. Biswas, J. S. Epstein, S. M. Feinstone, J. S. Finlayson, D. Tankersley, H. J. Alter, and J. H. Hoofnagle “Public Health Service Inter-Agency Guidelines for Screening Donors of Blood, Plasma, Organs, Tissues, and Semen for Evidence of Hepatitis B and Hepatitis C” *MMWR Recommendations and Reports* 40(RR-4), 1-17 (1991).
- [3] K. A. Aldwoah, Mohammed A. Almalahi and K. Shah "Theoretical and Numerical Simulations on the HBV Model through a Piecewise Fractional Order" *fractal and fractional* 7 844, (2023).
- [4] R. O. Aja, T. Chinebu, and G. C. E. Mbah, “Simulation on the mathematical model for the control of hepatitis B virus–hepatitis D virus (HBV–HDV) co-infection transmission dynamics in a given population,” *Journal of Mathematical Sciences and Modelling*, 4(2), 72–88 (2021).
- [5] Y. C. Chen, C. C. Chang, C. P. Lin, W. Y. Tsai, C. M. Yeh, T.-G. Kuo, and C.Y. Yeh, “Molecular epidemiology of hepatitis D virus infection among injecting drug users with and without human immunodeficiency virus infection in Taiwan,” *Journal of Viral Hepatitis*, 16(11), 807–816 (2009).
- [6] N. Gul, R. Bilal, E. A. Algehyne, M. G. Alshehri, M. A. Khan, Y. M. Chu and S. Islam "The dynamics of fractional order Hepatitis B virus model with asymptomatic carriers" *Alexandria Engineering Journal* 60(4), 3945–3955 (2021).
- [7] E. A. Hernandez-Vargas and R. H. Middleton, "Modeling the three stages in hepatitis B virus infection", *Journal of Theoretical Biology*, 320, 35–45 (2013).
- [8] S. A. Hughes, H. Wedemeyer and P. M. Harrison, "Hepatitis delta virus", *The Lancet*, 378(9785), 73–85 (2011).
- [9] I. Lenci, L. Tariciotti, R. Angelico, M. Milana, A. Signorello, T. M. Manzia, L. Toti, G. Tisone, M. Angelico, and L. Baiocchi, “Successful clinical and virological outcomes of liver transplantation for HDV/HBV-related disease after long-term discontinuation of hepatitis B immunoglobulins” *Clinical Transplantation* 37(6), e14971 (2023).
- [10] C. Castillo-Chavez and B. Song, "Dynamical models of tuberculosis and their applications", *Mathematical Biosciences*, 179, 21–35 (2004).
- [11] N. Chitnis, J. M. Hyman and J. M. Cushing "Determining important parameters in the spread of malaria through the sensitivity analysis of a mathematical model" *Bull. Math. Biol.* 70, 1272–1296 (2008).
- [12] N. Chitnis, J. M. Cushing and J. M. Hyman “Bifurcation analysis of a mathematical model for malaria transmission” *SIAP*. 67(1), 24–45 (2006).
- [13] R. Diyar, I. Ahmad, N. Ali, I. U. Haq, M. Idrees, and M. D. Albalwi, “A fractional order mathematical model for the Omicron: a new variant of COVID-19,” *Phys. Scr.* 99(11), 115255 (2024).
- [14] E. E. Endashaw and T. T. Mekonnen, “Modeling the effect of vaccination and treatment on the transmission dynamics of hepatitis B virus and HIV/AIDS coinfection.” *J. Appl. Math.* 5246762 (2022).

- [15] J. Fung, C. L. Lai, and M. F. Yuen, "Management of hepatitis B virus infection before and after liver transplantation: clinical and virological aspects", *Journal of Hepatology*, 34(4), 974–981 (2001).
- [16] L. Perko, *Differential Equations and Dynamical Systems*, 3rd ed., Springer, New York, 2013.
- [17] H. Kamal, R. Fornes, J. Simin, P. Stål, A.-S. Duberg, N. Brusselaers, and S. Aleman, "Risk of hepatocellular carcinoma in hepatitis B and D virus co-infected patients: a systematic review and meta-analysis of longitudinal studies," *J. Viral Hepat.*, 28(10), 1431–1442 (2021).
- [18] B. de Sousa and C. Cunha, "Development of mathematical models for the analysis of hepatitis delta virus viral dynamics," *PLoS ONE*, 5(9), 1–15 (2010).
- [19] C. Dietz-Fricke, F. Tacke, C. Zöllner, M. Demir, H. H. Schmidt, C. Schramm, K. Willuweit, and C. M. Willuweit, "Treating hepatitis D with bulevirtide — real-world experience from 114 patients" *JHEP Reports* 5, 100686 (2023).
- [20] A. J. Stockdale, "Hepatitis D," in *Comprehensive Guide to Hepatitis Advances*, Elsevier, Amsterdam, The Netherlands, 2023, pp. 281–307.
- [21] H. R. Joshi "Optimal control of an HIV immunology model" *Optim. Control Appl. Methods* 23(4), 199–213 (2002).
- [22] T. Khan, R. Ullah, G. Zaman, and I. Ahmad, "The analysis of hepatitis B virus (HBV) transmission using an epidemic model," *Nat. Appl. Sci. Int. J. (NASIJ)* 2(1), 70–79 (2021).
- [23] M. Khan, T. Khan, I. Ahmad, Z. Shah, and A. Khan, "Modeling of hepatitis B virus transmission with fractional analysis," *Math. Probl. Eng.* 2022(1), 6202049 (2022).
- [24] T. Kushner, B. Da, A. Chan, D. Dieterich, K. Sigel, and B. Saberi, "Liver Transplantation for Hepatitis D Virus in the United States" *Transplantation Direct* 8(1), e1253 (2022).
- [25] J. Li, Y. Yang and Y. Zhou "Global stability of an epidemic model with latent stage and vaccination" *Nonlinear Anal. Real World Appl.* 12(4), 2163–2173 (2011).
- [26] J. P. LaSalle, *The Stability of Dynamical Systems*, SIAM (1976).
- [27] J. Lou, J. Cheng, Y. Li, C. Zhang, H. Xing, Y. Ruan and Y. Shao "Comparison of different strategies for controlling HIV/AIDS spreading in MSM" *Infect. Dis. Model.* 3, 293–300 (2018).
- [28] J. Mann and M. Roberts "Modelling the epidemiology of hepatitis b in New Zealand." *J. Theor. Biol.* 269(1), 266–272 (2011).
- [29] T. T. Mamo and S. T. Tefera "A Mathematical Model Analysis of a Super Infection Control Strategy for the Hepatitis B–Hepatitis D Viruses in Highly Epidemic Areas of the World." *J. Math. Sci. Model.* 13(4) (2023).
- [30] P. Sanchez and D. Ramirez, "Limitations of interferon therapy for HDV," *Liver Transplant.*, 75–85 (2021).
- [31] H. Younas, I. Ahmad, N. Ali, I. U. Haq, M. D. Albalwi, S. Muhammad, and M. Shuaib, "Modeling rabies dynamics: The impact of vaccination and infectious immigrants on public health," *Contemp. Math.* 3255–3279 (2024).

- [32] T. E. Starzl, S. Iwatsuki, D. H. Van Thiel, J. C. Gartner, B. J. Zitelli, J. J. Malatack, R. R. Schade, B. W. Shaw Jr., T. R. Hakala, J. T. Rosenthal, and K. A. Porter, "Evolution of Liver Transplantation," *Hepatology*, vol. 2, pp. 614–636, 1982.
- [33] N. A. Terrault, C. Francoz, M. Berenguer and J. Heimbach, "Liver Transplantation 2023: Status Report, Current and Future Challenges" *Clin. Gastroenterol. Hepatol.* 21, 2150–2166 (2023).
- [34] A. J. Stockdale, S. Kreuels, A. Henning, "Hepatitis D prevalence: A global systematic review and meta-analysis" *Journal of Hepatology* 73(3), 523–532 (2020).
- [35] C. W. Shepard, E. P. Simard, L. Finelli, A. E. Fiore, and B. P. Bell, "Global epidemiology of hepatitis B virus infection", *The Lancet Infectious Diseases*, 6(6), 448–457 (2006).
- [36] World Health Organization, "Global Health Sector Strategies on HIV, Viral Hepatitis and the Sexually Transmitted Infections" *World Health Organization*, Geneva, Switzerland, pp. 2022–2030 (2021).
- [37] I. Ullah, I. Ahmad, N. Ali, H. Ahmad, and I. U. Haq, "Mathematical modeling and analysis of dynamics of Neisseria Gonorrhoea disease with self protection, treatment and natural immunity," *Glob. J. Sci.* 1(1), 40–55 (2024).
- [38] I. Ullah, N. Ali, I. U. Haq, I. Ahmad, M. D. Albalwi, and M. H. Ali Biswas, "Analysis of COVID-19 disease model: Backward bifurcation and impact of pharmaceutical and nonpharmaceutical interventions," *Int. J. Math. Math. Sci.* 2024(1), 6069996 (2024).
- [39] L. Zou, W. Zhang and S. Ruan, "Modeling the transmission dynamics and control of hepatitis b virus in china" *J. Theor. Biol.* 262(2), 330–338 (2010).
- [40] T. E. Chang, C. W. Su, Y. S. Huang, Y. H. Huang, M. C. Hou, and J. C. Wu, "Hepatitis D virus dual infection increased the risk of hepatocellular carcinoma compared with hepatitis B virus mono infection: A meta-analysis" *Journal of the Chinese Medical Association* 85(1), 30–41 (2022).
- [41] R. Zakh, A. Churkin, W. Bietsch, M. Lachiany, S. J. Cotler, A. Ploss, H. Dahari, and D. Barash, "A Mathematical Model for Early HBV and HDV Kinetics During Anti-HDV Treatment" *Mathematics* 9(24), 3323 (2021).
- [42] Hepatitis B Foundation, "Facts and Figures" *Hepatitis B Foundation* (2023).
- [43] M. Rizzetto, M. G. Canese, S. Arico, O. Crivelli, C. Trepo, F. Bonino and G. Verme, "Immunofluorescence detection of a new antigen-antibody system associated with hepatitis B virus in liver and serum of HBsAg carriers", *The Lancet*, 310(8030), 986–990 (1977).
- [44] M. A. Nowak and R. M. May, "Virus dynamics: Mathematical principles of immunology and virology", *Oxford University Press*, Oxford (2000).
- [45] B. C. de Sousa and M. V. Cunha, "A mathematical model for hepatitis B and D virus co-infection", *Mathematical Biosciences*, 225(2), 116–124 (2010).
- [46] A. S. Perelson, "Modelling viral and immune system dynamics", *Nature Reviews Immunology*, 2(1), 28–36 (2002).